Journal of Computing and Security

Research Article, 2021, Volume 8, Number 2 (pp. 43–57)

http://www.jcomsec.org

Scalability Analysis of a LoRa Network Under Inter-SF and Co-SF Interference with Poisson Point Process Model

Solmaz Mohammadi [a], Gholamreza Farahani [a,*]

[a] *Department of Electrical Engineering and Information Technology, Iranian Research Organization for Science and Technology (IROST), Tehran, Iran.*

ARTICLE INFO.

Article history:
Received: 10 August 2021
Revised: 10 November 2021
Accepted: 13 December 2021
Published Online: 17 January 2022

Keywords:
Scalability of LoRa, LoRaWAN, Inter-SF and Co-SF Interference, Coverage Probability, Success Probability.

ABSTRACT

The scalability of a single gateway LoRa network depends on different parameters such as interference and noise. The scheme of spreading factor allocation can control the interference and noise. This article analyzes the impact of the interference of the concurrent transmission with the same spreading factor (co-SF) and different spreading factor (inter-SF) on the scalability of the LoRa network. The interference has been modeled as the Poisson point process. The proposed scheme considers the success probabilities and device density (SPD) in each area in determining the width and boundaries of SF areas. The simulation results showed that the proposed SPD scheme had improved 13.20% over the EIB method in terms of success probability under joint co-SF and inter-SF interference. Also, the coverage probability under the joint impact of cumulative co-SF and inter-SF interference of the SPD and EIB methods is compared in the clean and noisy conditions. The probability of coverage in EIB degrades more than SPD as the scalability increases. Also, the uplink performance of the proposed SPD scheme has been studied in the absence of any interference under AWGN. SPD has a higher success probability under AWGN than EIB.

© Research Article, 2021 JComSec. All rights reserved.

1 Introduction

Internet of things (IoT) technology has utilizations in agriculture, transportation, smart buildings, and smart cities. With the exponential growth of global data volume and the continued improvement of IoT, and the popularity of connected devices, IoT devices must consume low power and be reliable and scalable [1].

For long-range scenarios, 3G, long-term evolution (LTE), and 5G technologies support the IoT applications [2]. The low power wide area network (LPWAN) technology was preferred for IoT applications when the GSMA launched the mobile IoT in a series of LPWAN standards to accelerate the commercial availability. It refers to a class of network technologies designed for wireless communications over long distances using lower energy and cost. LPWAN is essential for the extension of IoT networks in terms of their connectivity infrastructure. The public LPWAN technologies are LoRa, narrow band-IoT (NB-IoT) [3], and SigFox [4]. Among them, LoRa has become more attractive since its open-source standards have made it possible to construct an individual network at a lower cost [5].

* Corresponding author.
Email addresses: s.mohammadi@irost.org (S. Mohammadi), farahani.gh@irost.org (G. Farahani)
https://dx.doi.org/10.22108/JCS.2021.129691.1073
ISSN: 2322-4460 © Research Article, 2021 JComSec. All rights reserved.

The long-range (LoRa) alliance is for low power, low bandwidth, and low latency applications [6].

LoRa wide area network (LoRaWAN) is an LPWAN standard and open media access control (MAC) protocol developed by LoRa Alliance [7]. The devices connect to the gateway or base station via a one-hop link by pure-ALOHA in a LoRaWAN network in a star topology type. Pure ALOHA is prone to collisions since it has no competitive mechanism [8].

LoRa defines the physical layer with parameters, namely spreading factors (SFs), bandwidth (BW), carrier frequency offset (CFO), and coding rate (CR) [9]. The BW demonstrates the frequency range at which the devices will communicate. CFO indicates the frequency offset. CFO occurs due to subtle differences between the carrier frequency of the transmitter and receiver. The CR shows the proportion between the number of packet payload bits and the bit length of the error correction code. A lower CR increases packet length but gives stronger protection from error. The SF defines the ratio of the chip rate to the symbol rate. The increase in SF enhances the sensitivity and communication range and raises the time on-air. LoRa utilizes the chirp spread spectrum (CSS) radio modulation. LoRa uses orthogonal SFs for transmission. Different SFs have different chirp rates, which change in frequency with time. Because CSS uses frequency chirps with linear frequency changes over time, the chip rate will be the slope of the line when plotting frequency versus time that provides different slopes, and these slopes provide orthogonality property [10]. Signals modulated with orthogonal SFs and transmitted simultaneously through the same channel don't interfere with each other. Therefore, packets can be received concurrently and increase the number of deployed end devices. Thus, orthogonal SFs determine the deployment scalability of devices [11].

It has proved that, under some circumstances, such as low Signal-to-Noise Ratio (SNR), SFs are not perfectly orthogonal; therefore, they are imperfect orthogonal [12]. The effects of this imperfect orthogonality have been indicated that depend on: (i) the specific LoRa transceiver, (ii) perceived SNRs, and (iii) the number of deployed end devices [13].

Additionally, this allows the network to maintain the battery lifetime of the end devices by creating adaptive optimizations of the power level and data rate. LoRa made a trade-off between data rate and sensitivity while working in a fixed bandwidth of 500 kHz (for downlink) and 125 kHz or 500 kHz (for uplink). Sensitivity is a value for determining the device's capacity to detect a weak signal.

The allocation of the spreading factor is an effective parameter for the scalability of networks. Interference in LoRa is divided into inter-SF and co-SF interferences. The LoRa scalability is dependent on the same spreading factor (co-SF) and different spreading factor (inter-SF) interferences. Inter-SF interference may result from imperfect orthogonality among different SFs and indicates that the transmissions with different SFs are not completely safe and secure against neighbor SFs. Therefore, a specified level of signal-to-interference ratio (SIR) protection is necessary [14]. If the SIR is below a specified threshold, the scalability is destroyed. Co-SF interference has resulted from irregular same channel transmissions using the same SF. It can limit the scalability in high-density deployments if the SIR in the transmission is below a specified threshold.

In this paper, the LoRa scalability has been analyzed under imperfect-orthogonality of SFs with the impact of varying parameters such as SF. The Poisson point process is chosen for modeling the interference field under the improved ALOHA protocol. The proposed scheme in this article is a success-probability-based algorithm that is computed under the joint impact of concurrent transmissions that use co-SF and inter-SF interference. SF-allocation is carried out by a multi-annulus structure which is specified by the success probability of annuluses and device density at the beginning of configuration. It will prove that considering the success probabilities in allocating the SFs to devices degrades inter-SF and co-SF interference and positively affects noise conditions.

To assess the performance of the proposed method in the existence of simultaneous uplink transmissions, success probability and coverage probability in the presence of inter-SF and co-SF interference will be computed. In addition, these metrics will be calculated in the existence of background additive white Gaussian noise (AWGN) conditions to evaluate the performance of the uplink transmission.

Other sections of the paper are organized as follows. Section 2 reviews related works in LoRa scalability. In Section 3, the LoRa and LoRaWAN are described. Section 4 explains the system, channel, and signal models. Section 5 presents the compared EIB method in allocating SFs for evaluating scalability. Section 6 describes the modeling of the interference field as a Poisson point process and defines the interference-free environment in the presence of AWGN. Section 7 introduces the proposed scheme. The results of simulations and discussion are given in Section 8. Finally, the conclusions are stated in Section 9.

Date and location of the research: July 2021, an Iranian research organization for science and technology (IROST).

2 Related Work

LoRa has different Challenges with scalability that are derived from different factors as below [15]:

- The number of end devices exceeds the gateway capacity in the absence of synchronization between gateway and end devices.
- All devices with a gateway utilize the same channels for uplink transmissions.
- Time on-air can be large, normally is within a few seconds.
- The pure-ALOHA MAC layer is used for uplink transmissions.
- All gateways have transmissions "off the air" without receiving an acknowledgment from the end devices to know they intend to transmit or not.

Different procedures of scalability optimization, such as compressed acknowledgments, synchronous-slotted of uplink transmission, dynamic transmit power, frequency block hopping, and SF selection, quality of service, and listen before the talk method for MAC layer can be performed. To access scalability in LoRa, success connectivity is necessary for a massive number of end devices. Lora provides parameters including CR, BW, and SF. Utilizing the same parameters grows the probability of collisions. Some researchers have suggested SF optimization schemes. Optimization of SFs can improve the success probability of packet exchange as well as reduce node energy consumption. In [13], the accessible throughput has been analyzed theoretically in uplink transmission, including the capture conditions of LoRa. The conclusion was that imperfect orthogonality of SF under different SF-allocation has a non-negligible impact on the throughput losses. This research proved that the SFs are not completely orthogonal. It has been shown the interference effects on communication in the LoRa network. There are little researches that consider the complete orthogonality between SFs. In [14], the authors have analyzed link-level in the LoRa network with regard to the imperfect-orthogonality imperfect impact of the SFs. As imperfect-orthogonality exists between SFs, LoRa cell works on independent channels. When the interfering power is enhanced, the received signal cannot be demodulated properly. Croce et al. [14] presented that inter-SF collisions are a main problem in the LoRa cells.

Assigning higher SFs to devices away from the gateway may not necessarily increase their link capacity. Lim et al. [16] assigned the SF based on the distance between the end device and gateway. They developed a mathematical model to select an optimal distance for SF-allocation. This model includes inter-SF interference and co-SF packet collision. Three procedures are used in [17] to allocate SFs to end devices, including fixed SF, random SF, and packet loss ratio-based SF. The constant SF-allocation assigns the same SF to all the end devices at the configuration of the network. The random SF method assigns SFs to end devices randomly. The packet loss ratio-based SF assigns the lowest probability SF based on packet loss ratio, and this approach outperforms both random and fixed SF allocation.

An SNR-based SF-allocation method has been proposed by Georgiou et al. [18] for raising the scalability in LoRaWAN. An analytical framework is developed using stochastic geometry. In this method, SF in each annulus is determined due to SNR, and the success probability of the packet considering the inter-SF and co-SF interferences has improved.

About the downlink performance of LoRa for scalability development, one limitation is the inadequate capacity in the downlink, which results in unreliable communication between devices. Vincenzo et al. [19] presented a method related to scalability problems concerning the downlink traffic and proposed solutions to use acknowledgments for low to medium downlink load. A method including two mechanisms is proposed for downlink transmission to improve the LoRa network scalability in [20]. This method reduces the uplink transmission outage by decreasing the downlink time and choosing downlink time according to uplink time; as a result, it serves more end devices and improves scalability.

The LoRa network's scalability is dependent on the SF-allocation methods. Saluja et al. [21] proposed an exponential windowing scheme (EWS) for LoRa, an SF allocation method based on distance. A distance parameter is allocated to each SF to increase the success probability under co-SF interference of the overall LoRa network.

Link budget and channel collision have a direct impact on scalability. In [22], Cai et al. proposed an orthogonal genetic algorithm based on dynamic parameter selection. Each end device chooses its parameter settings according to the budget link, minimizes the collision probability, and enhances scalability.

In other researches, the scalability of the network is determined by the media access type, the schemes such as time-slotted MAC, pure ALOHA, and slotted ALOHA. LoRaWAN MAC protocol based on ALOHA constraints the reliability and scalability. The utilization of time-slot communications is a popular method to improve scalability in wireless networks. Even if the end devices are very randomly deployed, a good MAC will assure an absolute spacing between simultaneous interferers. To enhance the scalability and the single-channel capacity in LoRa networks, Poloneli

et al. [23] suggested a regulated or slotted ALOHA (S-LoRaWAN) for LoRaWAN communication which is the synchronization-based service. S-LoRaWAN increases the performance of popular LoRaWAN with regard to the network throughput and packet collision rate. S-LoRaWAN has low overhead in the downlink, and as a result, it consumes less energy. One of the issues being discussed is the impact of the capture effect on scalability. In this case, Reynders et al. in [24] presented the RS-LoRa MAC layer to analyze and progress the LoRaWAN scalability and reliability with lightweight scheduling to assume devices into the category in which equivalent transmission powers has been utilized in each category to decrease the capture effect. Coarse-grained scheduling of nodes will carry out by a gateway through dynamically determining the provided SFs and transmission powers on each channel. The end device determines its SF, transmission power, channel, and transmitting timing to perform concurrent sending. Therefore, it reduces packet collisions and increases network reliability and scalability.

A specific method for class A end devices, a synchronization, and a scheduling method for LoRaWAN was proposed by Haxhibeqiri et al. [25]. This scheme can be implemented on the existing LoRaWAN MAC. A scheduler and synchronizer plan downlink and uplink transmissions of devices. Each node should request time slots from the scheduler for sending, which decreases the synchronization packet length, sends more information towards the end device, and positively affects scalability.

3 LoRa and LoRaWAN

In the following, LoRa technology is introduced, consisting of two parts: LoRa physical layer modulation and LoRaWAN MAC layer. The LoRa network has a stratified structure in which the end devices are connected through LoRa physical layer to the gateway [26]. Modulation of LoRa is CSS-based and transmits a chirp signal. All chirps have equal durations, in which the modulator produces different chirps with specified time-shift compared to the primitive chirp for digital inputs. LoRaWAN is an open-source protocol that describes the MAC layer protocol and network architecture to communicate multiple devices and their gateways. Equipment defined by LoRaWAN is end devices, gateway, application server, and network server. The network server controls the network, decodes the packets, parameter allocation such as bandwidth or SFs, and authentication. Application servers accept end devices on the network and oversee encryption or decryption. The gateways are responsible for transmitting LoRaWAN packets of nodes and forwarding them to the network server. The network server sends downlink packets towards end devices.

The LoRaWAN doesn't know the contents of packets, as it has transmission at bit level. Three types of nodes have been defined for the LoRaWAN requirements: class A, class B, and class C [27]. End devices in the rank of class A have bidirectional communication, in which two receive windows follow the single uplink transmission window. The subsequent downlink transmission waits until the uplink transmission is performed.

Among the three classes, class A has the least energy consumption. Class B is also bidirectional. Its end devices open an additional receiving window in the scheduled time. In this class, the network server knows when the end device is in listening mode with a synchronized beacon of the gateway. Bidirectional class C has a maximum receive slot. Class B end devices consume the most energy because they have continuous receive windows.

The LoRa physical modulation is scalable either in frequency or bandwidth, creates bidirectional communication that spreads the narrow bandwidth signal within a large bandwidth to increase the receiver sensitivity and make a robust signal against noise and interference. Multiple chips of information represent each information bit. As the spread factor is higher, the number of chips per symbol will be higher. Therefore, the data rate decreases. Six SFs, from 7 to 12, are used that are orthogonal. The number of chips in each symbol is defined by 2^{SF}.

The use of multiple SFs and transmission channels results in a superposition of independent subsystems. The SFs in LoRa is quasi orthogonality. Quasi-orthogonality has relevance with parameters such as SFs. Quasi-orthogonal signals have an action similar to a virtual channel using changing duration of chirp. The modulated signal is very resistant to interferences and AWGN. Low SFs result in a low quasi-orthogonality.

4 The Channel, Signaling, and System Model

4.1 System-Level Modeling

This section presents the architecture, assumptions, and specifications of the deployed network. N is the number of end devices deployed randomly with a single gateway in a 2-D space model. The gateway is supposed that be fixed. S is the region of deployment that is assumed as a circle with radius R. Containing area of devices is $A = |S| = \pi R^2$. The number of devices has a Poisson random variable distribution with intensity $\lambda > 0$ and mean $\overline{N} = \lambda A$ same as assumed in [12]. For the random technique, the locations of

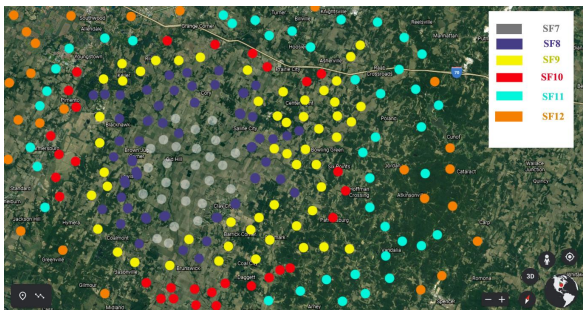

Figure 1. Practical Deployment and Real Condition of SF Allocation.

end devices substitute the time instants, and the path loss model is the impulse responses of time instants, described in subSection 6.1.

To uplink transmitting, end devices utilize the ALOHA protocol. Each device has a processor that can work with a network server to obtain the SF. End devices transmit utilizing an omnidirectional antenna from all directions, and their constant transmission power of signals is p_t. Transmissions are carried out in the same channel with bandwidth B. The outage probability complements the success probability of receiving and demodulating packets correctly. The outage and success probability depending on two interference are determined in uplink transmission, inter and co-SF interferences.

The inter-SF interference arises when simultaneous transmissions happen from all designated areas with devices that use quasi-orthogonal SFs [28]. In contrast, co-SF interference results when the packets are sent simultaneously with the identical SF.

Transmissions interfere at the gateway with the desired transmission regions. Under realistic circumstances, there are no precise boundaries for SFs regions, as shown in Figure 1.

4.2 Channel and Signal Model

The inter-SF transmissions are less disruptive than co-SF transmissions because they need a lower SIR threshold. For practical analysis, the influence of inter-SF interference has been considered. Theoretically, LoRa covers a long range of ten kilometers. Its performance drops after two or three kilometers and is highly affected by inter-SF and co-SF interference or AWGN noise. Assume a device x_1 that is placed in the i-th annulus; when this device communicates with the gateway, the other devices in all of the areas act as an interferer. The received signal $r_1(t)$, with the existence of inter-SF and co-SF interferences, can be given as (1):

$$r_1(t) = l(x_1)\, h(t) \times s_1(t, SF_p) + \sum_{j=2}^{N_{SF_p}} 1_k^{SF_q} l(x_j)\, g_j(t) \times s_j(t, SF_p) + \sum_{q \in \kappa \setminus p} \left(\sum_{k=1}^{N_{SF_p}} 1_k^{SF_q} l(x_k)\, g_k(t) \times s_k(t, SF_q) \right) + n(t) \quad (1)$$

where $s_1(t, SF_p)$ is the transmitted signal with spreading factor parameter SF_p, $h(t)$ is the immediate fading coefficient which is a zero-mean circularly symmetric complex Gaussian (CSCG) random variable with unit-variance [12]. Unit-variance means $E[|h|^2] = 1$, which relates to Rayleigh fading. Transmissions were carried out with AWGN over the Rayleigh fading in the channel. Assume $s_i(t, SF_q)$ is the interfering signal of device i at spreading factor over the Rayleigh block-fading channel with fading coefficient $g(t)$, $n(t)$ is AWGN with variance $\sigma^2 = N_0 + NF + 10\log_{10} B[dBm]$ and zero mean, NF is the noise figure of the receiver which is fixed, and N_0 is the noise power density, B is the bandwidth of the channel, $1_i^{SF_x}$ is an indicator function of device i that transmits at SF_x, N_{SF_x} is the number of end devices that use SF_x, $\ell(x_i)$ is the path loss function, and x_i is the distance of device i away from the gateway [29].

5 EIB Scheme

The different levels of signal attenuation may happen for the generated signals by end devices because of interference, path loss, and shadowing. This issue can be handled using specifying and varying SFs assigned to the end devices. The equal-interval-based (EIB) scheme [12] assumes a simple equal-width multi annulus for scalability analysis. The method also assumes the effect of inter-SF and co-SF interferences from imperfect orthogonality of signals at different SFs to calculate the success probability and estimate scalability. This method works better than the path-loss-based method. EIB uses stochastic geometry to model the interference, which is a powerful stochastic network behavior model [30]. It finds a stochastic mean of inter-SF and co-SF interferences power by summing interference transmissions. A shot noise process is used for modeling the interference. The noise components are considered as Poisson distributed time instants [31]. For a stochastic spatial process, the spatial locations of nodes are utilized with the path loss model.

The success probabilities are computed for the joint impact of inter-SF and co-SF interferences resulting from the concurrent transmission.

6 The Interfering and Noisy Environment

6.1 Poisson Distribution Modeling of the Interference

Interference is the important limiting factor of the performance in the LoRa network. It is essential to define interference statistics. In the network, while transmitting the signal from an end device, other devices are considered interferers. Therefore, interferer distribution can be modeled as stochastic geometry models.

One of the device distribution models is the Poisson point process. ALOHA has inherent matching with the Poisson point process because ALOHA keeps its properties. In addition, because of the superposition feature of the Poisson point process, the interference is proportional to density. The Poisson point process is easy to analyze because of the independence property. From a practical aspect, the Poisson point process is suitable when many devices are distributed randomly. Most large-scale wireless networks are deployed randomly; for example, large numbers of devices fall from aircraft or move independently in an area. While interference characterization is related to large networks, it is the same as shot noise. To analyze the uplink transmission, if the interferers have been distributed due to a stochastic point process, the inter-SF and co-SF interferences are modeled as a random field or a shot noise procedure [30]. In general, shot noise is measured in time; the points in the Poisson point process are time instants. Basic shot noise is defined as: $I(t) = \sum_{i=1}^{\infty} g\left(t - x_i\right)$. To model interference, the time axis will be substituted by the spatial axes, and the impulse response $g(x)$ will also be replaced by the path loss function $\ell(x)$.

The noise components are assumed to be the Poisson distribution of time instants. At each time moment of sampling, the locations of the interferers or end devices are supposed to be distributed in which for the spatial point process Π with intensity λ , time moments are substituted with different spatial locations of the interferers. In multi-dimensional point processes, a shot noise process $I(y)$ with stochastic impulse response is described as (2) [32]:

$$I(y) = \sum_{x \in \varphi}^{\infty} K_x g(y - x) \tag{2}$$

where K_x are the same and independent distributed stochastic variables that can be used to model fading, $g(y - x)$ is the impulse response, and φ is a point process of interferers on $\mathbb{R}^d$. The total interference power I_a measured at the origin, given by (3):

$$I_a = \sum_{x \in \varphi \cap b(o,a)} \ell(x) \tag{3}$$

$\varphi \cap b(o, a)$ is a finite point process for the free space path loss for an i-th end device located at x distance from the gateway in which the interference from the devices located within the distance a of the origin, x is the Euclidean distance of the device i from the gateway, and $\lim_{x \to \infty} \ell(x) = 0, \ell(x)$ is the path loss function.

For the standard power law, the path loss law is defined as $\ell(r) = r^{-\eta}$. $\mathcal{F}_{I_a}(\omega)$ is Fourier transform of I_a and assuming $a \to \infty$, $I_a = I$, $\mathcal{F}_{I_a}(\omega)$ becomes $\mathcal{F}_I(\omega)$, for $\eta > 2$ yields:

$$\mathcal{F}_I(\omega) = \exp\left(-\lambda \pi \Gamma(1 - 2/\eta)\omega^{2/\eta} e^{-j\pi/\eta}\right), \omega \geq 0 \tag{4}$$

where η is the path loss exponent, ω is the angular frequency, and $\Gamma(p)$ is the standard gamma function by the definition of $\Gamma(p) \triangleq \int_0^{\infty} t^{p-1} e^{-t} dt$.

6.2 Uplink Performance in the Clean and AWGN Conditions

When the SNR of the received signal drops under the threshold, denoted by θ_{SF} an uplink outage of the signal occurs. In this case, for the noise-limited environment in which interference is absent, the outage of the AWGN channel will be evaluated. Assume $H = |h|^2$ is the channel gain between the end device and the gateway; therefore, due to (1) the SNR is denoted as (5):

$$SNR = p_t H l\left(x_1\right) / \sigma^2 \tag{5}$$

where p_t is the transmitting power of the node and H is an exponential random variable. The success probability under AWGN of a device P_{SNR} with distance x_1 from the gateway is as (6):

$$P_{SNR}\left(x_1, \theta_{SF}\right) = \exp\left(\sigma^2 \theta_{SF} / p_t l\left(x_1\right)\right) \tag{6}$$

where θ_{SF} remains constant for each annulus. The SF-dependent SNR thresholds due to Semtech [33] are given in Table 1.

In the following, the success probability and coverage probability are obtained by considering the impact of joint inter-SF and co-SF interference in the clean and AWGN conditions.

Table 1. THE SF-Dependent SNR Thresholds.

Annulus	SF	SNR threshold $(\theta_{SF})(dB)$
1	7	-6
2	8	-9
3	9	-12
4	10	-15
5	11	-17.5
6	12	-20

6.3 SIR-Based Probability of Success Under Joint Inter-SF and Co-SF Interference

This section analyses the success probability of a signal under the joint effect of inter-SF and co-SF interferences. This evaluation metric determines how inter-SF and co-SF interferences affect the performance. LoRa layer is assumed as a protocol without retransmission of packets; in addition, the devices transmit independently of others.

Considering fixed environment conditions, assume a device in density annulus i at a distance x_1 away from the gateway, the success probability in the existence of the inter-SF and co-SF interferences P_{SIR}^{Π} is calculated according to (7) and (8) as:

$$P_{SIR}^{\Pi}\left(x_1, \delta_{ij}\right) = \exp\left(-2\pi\alpha\lambda \sum_{j=1}^{k} I\left(x_1, \delta_{ij}, \{\ell_{j-1}, \ell_j\}\right)\right) \tag{7}$$

where

$$I\left(x_1, \delta_{ij}, \{\ell_{j-1}, \ell_j\}\right) = \int_{\ell_{j-1}}^{\ell_j} \frac{\delta_{ii} l(x)}{l\left(x_1\right) + \delta_{ii} l(x)} x dx \tag{8}$$

and $\delta_{ii}[dB]$ is the required threshold for the received signal SF_i upon active interferers transmitting at the same SF_i. $\delta_{ij}[dB]$ denotes the threshold required for the desired signal SF_i against interferers that employ the SF_j which is presented at matrix that is given as (9) [34]. $\alpha\lambda$ is density due to independent thinning of the homogeneous Poisson point process of end devices or density of modeled field. ℓ_{j-1}, ℓ_j are boundaries of the annuluses in which the devices have the same SF_j.

$$\Delta_{[dB]} = \begin{array}{c} \\ SF7 \\ SF8 \\ SF9 \\ SF10 \\ SF11 \\ SF12 \end{array} \begin{array}{c} \begin{array}{cccccc} SF7 & SF8 & SF9 & SF10 & SF11 & SF12 \end{array} \\ \begin{bmatrix} 1 & -8 & -9 & -9 & -9 & -9 \\ -11 & 1 & -11 & -12 & -13 & -13 \\ -15 & -13 & 1 & -13 & -14 & -15 \\ -19 & -18 & -17 & 1 & -17 & -18 \\ -22 & -22 & -21 & -20 & 1 & -20 \\ -25 & -25 & -25 & -24 & -23 & 1 \end{bmatrix} \end{array} \tag{9}$$

6.4 Coverage Probability Under Inter-SF and Co-SF Interference

The coverage probability is the probability that each device is in coverage and accessible for the gateway (hasn't outage). It can successfully communicate under inter-SF and co-SF interferences and even collision conditions at every specific moment. The coverage probability P_c can be achieved by averaging the distance distribution $f_D(x_1)$ and radius x_1. Uplink transmission of LoRa has a dual necessity that breaks up SIR and SNR [18]. The coverage probability $P_c[P_{SIR}^{\Pi}]$ is given in [35] by considering joint inter-SF and co-SF interference as (10).

$$P_c\left[P_{SIR}^{\Pi}\right] = \int_{d>0}^{R} P_{SIR}^{\Pi} \cdot f_D\left(x_1\right) dx_1 \tag{10}$$

The coverage probability per annulus i, $P_{c,i}[P_{SIR}^{\Pi}]$ is as (11):

$$P_{c,i}\left[P_{SIR}^{\Pi}\right] = \frac{2}{\left(\ell_{i+1} - \ell_i\right)^2} \int_{\ell_i}^{\ell_{i+1}} P_{SIR}^{\Pi} P_{SIR}^{\Pi} \cdot x_1 dx_1 \tag{11}$$

The coverage probability for the assumed region of the LoRa network with respect to P_{SIR}^{Π} is as (12).

$$P_c\left[P_{SIR}^{\Pi}\right] = \frac{2}{\left(\ell_{i+1} - \ell_i\right)^2} \sum_{i=0}^{n} \int_{\ell_i}^{\ell_{i+1}} P_{SIR}^{\Pi} \cdot P_{SIR}^{\Pi} \cdot x_1 dx_1 \tag{12}$$

6.5 Joint Coverage Probability

Signal-to-interference-plus-noise ratio (SINR) based coverage probability or joint coverage probability $P_c[P_{SIR}.P_{SIR}^{\Pi}]$ demonstrates how interference and AWGN degrade the LoRa scalability. Co-SF interference is denoted by I_{co-SF} as (13).

$$I_{co-SF} = \sum_{x \in N} P_x \kappa \left|x_i\right|^{-\eta} \tag{13}$$

where η denotes the path loss exponent, $|x_i|$ is the Euclidean distance of LoRa devices to the gateway, P_x is the transmit power of the interference, $\kappa = (\lambda_c/4\pi)^2$, $\lambda_c = c/f_c$, f_c is the carrier frequency and c approximately equal to $3 \times 10^8 m/s$.

The inter-SF interference from LoRa nodes in other annuluses $I_{inter-SF}$ is given as (14).

$$I_{\text{inter }-SF} = \sum_{y \in G_y} \sum_{x \in N} P_x \kappa \left|y_i + x_i\right|^{-\eta} \tag{14}$$

where $|y_i + x_i|$ refers to the distance between the interferer with different SFs and gateway, G_y is the number of devices with different SF from the assumed device's SF in other annuluses, and N is the number of active devices with the identical SF in the same annulus.

The joint coverage probability is that each device can successfully communicate, and its signals are decoded at the gateway with a pre-defined SINR threshold. The joint coverage probability $P_{cov}(y_{th})$ is given by (15).

$$P_{\text{cov}}\left(\gamma_{th}\right) = E_R[PR[\text{SIN}\, R(R)]] \geq \gamma_{th}[R] \tag{15}$$

where R is the distance between the desired end device and the gateway, and E_R is the mathematical expectation. At a gateway, the received SINR for the LoRa device can be defined as (16).

$$SINR = \frac{P_x l\left(x_i\right)}{I_{co-SF} + I_{\text{inter }-SF} + \sigma^2} \tag{16}$$

where l_{x_i} is the path loss function as stated before, and is equal to $k|x_i|^{-\eta}$.

SINR thresholds for different SFs are given in the SINR matrix as (17) [36].

$$\gamma_{th} = \begin{array}{c} \\ SF7 \\ SF8 \\ SF9 \\ SF10 \\ SF11 \\ SF12 \end{array} \begin{array}{c} \begin{array}{cccccc} SF7 & SF8 & SF9 & SF10 & SF11 & SF12 \end{array} \\ \begin{bmatrix} 6 & -16 & -18 & -19 & -19 & -19 \\ -24 & 6 & -20 & -22 & -22 & -22 \\ -27 & -27 & 6 & -23 & -25 & -25 \\ -30 & -30 & -30 & 6 & -26 & -28 \\ -33 & -33 & -33 & -33 & 6 & -29 \\ -36 & -36 & -36 & -36 & -36 & 6 \end{bmatrix} \end{array} \tag{17}$$

Based on (15) and (16), the joint coverage probability $P_c[P_{SNR}.P_{SIR}^{\Pi}]$

$$\begin{aligned} P_c\left[P_{SNR} \cdot P_{SIR}^{\Pi}\right] &= PR\left(\text{SINR}(R) \geq \gamma_{th}\right) \\ &= PR\left\{\frac{P_x l\left(x_i\right)}{I_{co-SF} + I_{\text{inter }-SF} + \sigma^2} \geq \gamma_{th}\right\} \\ &= e^{-\rho\sigma^2}\, \mathrm{L}_{I_{co-SF}}(\rho) \mathrm{L}_{I_{\text{inter }-SF}}(\rho) \end{aligned} \tag{18}$$

where $\rho = R^{\eta}\gamma_{th}/P_x k$, $L_{I_{co-SF}}(\rho) = E\{e^{-\rho I_{co-SF}}\}$ and $L_{I_{inter-SF}}(\rho) = E\{e^{-\rho I_{inter-SF}}\}$ are the Laplace transforms of the power density distributions of interferences.

7 Proposed SPD Method

The proposed success probabilities and device density (SPD) method assume the six annuluses, wherein end devices have similar SF for each annulus. The area of annulus i is determined by $a_i = \pi r_i^2(2i-1)$ edges ℓ_{i-1} and ℓ_i, and radius $r_i = \ell_i - \ell_{i-1}$. ℓ_{i-1} and ℓ_i are the boundaries of an annulus with the formula $r_i = \ell_i - \ell_{i-1}$. According to Table 1, annulus i varies from 1 to 6 due to SF 7 to SF 12. Annulus 1 with the radius r_1 has boundaries ℓ_0 and ℓ_1, and starts from the location of the gateway, as a result, $\ell_0 = 0$ and $r_1 = \ell_1$. This method diminishes the packet error at the configuration time and increases the final success and coverage probability. Indeed, SPD reduces the impact of interferences and even AWGN on signal transmission. In the existence of only interference, the SIR of the received signal must be above the threshold. The impact of overall interference, *i.e.* real condition containing both inter-SF and co-SF, is almost equivalent to the power of interfering related to the interferer on the success probability of the concurrent uplink transmission from devices with the same or different SF. SPD assumes the division of the rings at the initialization phase as an equal interval (considering annuluses with equal width). In the next operation, the success probability with considering the inter-SF and co-SF interference is computed at

the first running of the network. After measuring the success probability under the joint impact of inter-SF and co-SF interference (P_{SIR}^{Π}) due to (7) and (8), then coverage probability $P_c[P_{SIR}^{\Pi}]$ with respect to (12), the specified SF for each annulus is computed based on obtained success probabilities at each iteration. If the success probability of annuluses is degraded, the annulus width will be reduced. Also, the density impacts and limits of the iteration are stated below.

For this purpose, the total density of the LoRa cell environment and the density of each annulus must be calculated. Generally, about the relation between the SF region width and density, it is mentioned that the end devices in the region near each other or dense case of the devices will most likely transmit packets simultaneously. Thus, their success probability is lower, and the annulus width should be decreased according to specific calculations. Consequently, computation of each annulus's density is essential to reduce the effect of interference and noise. In a high-density annulus, collisions and interference are more similar. As a result, in each annulus, if the interferences are higher than a threshold value, according to the probability obtained, SF zoning will perform at the network configuration. The device density of each annulus ρ_j is as (19):

$$\rho_j = N_{\ell_{i-1},\ell_i} / S_{\ell_{i-1},\ell_i} \tag{19}$$

where N_{l_{i-1},l_i} is the number of end devices in annulus j and S_{l_{i-1},l_i} is the area of annulus j. Practically, a smaller radius is associated with a higher density of annulus, and each annulus with a lower density gets wider. Hence, the density impacts the changing of the annuls' radius expressed as follows.

Assume $J = \{j \in N | 7 \leq j \leq 12\}$ is the vector of annulus's index concerning SF. First, the probabilities are calculated using (7) and (8). Annulus j has the minimum success probability, and coverage probability under inter-SF and co-SF interferences in each iteration m is defined as (20).

$$\begin{aligned} &\exists j \in J : j \notin C : P_{SIRj}^{\Pi} = \left(P_{SIR}^{\Pi}\right)_{\min}, \\ &P_c\left[P_{SIR}^{\Pi}\right]_j = \left(P_c\left[P_{SIR}^{\Pi}\right]\right)_{\min} \end{aligned} \tag{20}$$

Then the width of annulus j is decreased as (21) compared to the previous round. This value is added to the width of the inner annulus $j-1$

$$(r_j)_{m+1} = (r_j)_m - \gamma_j \tag{21}$$

$$(r_{j-1})_{m+1} = (r_{j-1})_m + \gamma_j \tag{22}$$

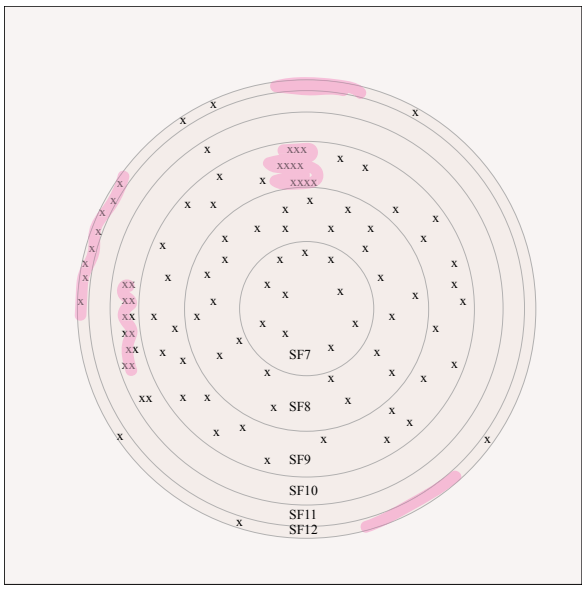

Figure 2. Allocation of SFs with SPD method, the devices are marked x around the gateway.

where $\gamma_j = \rho_j/\lambda$, m is the iteration number and r_j is the radius of the annulus $j \in J$. γ_j makes this reduction regarding the width and the number of devices in the interaction between the density of each annulus and the overall density. At the end of the iteration, changed annuluses are stored in vector C as (23).

$$c_p = j, c_{p+1} = j-1, c_p, c_{p+1} \in C \tag{23}$$

C is the vector that stores the index j of changed annuluses in each iteration and will reset in the next iteration. If $\rho_j > \lambda/3$, r_j is fixed and the process of increasing and decreasing for annulus j will stop.

The iterations loop repeats until the success probability of each annulus are more than 0.4 unless the ρ_j of that annulus is one-third of the total density. As the simulations are shown in Section 8, even in higher SFs, the success probability under joint cumulative inter-SF and co-SF is almost greater than 0.4.

This process starts from the annulus j with minimum $(P_{SIR}^{\Pi})_{min}$ and continues with the annulus $j+1$. SF7 has more width since it is proved in [12] that the less SF (*i.e.* SF7) has the higher probability of success because of the less interference. These steps are repeated until the success probability of each annulus is more than 0.4 to get the desired result.

In the next phase, another solution can be adopted. Thus, after carrying out the designation of success-probability-based annulus boundaries, the special devices are selected. Special devices are positioned in dense regions and are the least likely to succeed in transmitting. Special devices are chosen randomly

Algorithm 1 BB-Baseline Model Pseudo-Code.

Initialization step: selecting the annuluses widths based on the equal-interval-based method, assigning the SFs from 7 to 12 (from inner to outer annulus)
m=iteration (in this paper m_{max} =100);
while until $(P^{\Pi}_{SIR_j}) > 0.4$ or m = m_{max} **do**
  Calculating $(P^{\Pi}_{SIR_j})$ with respect to (7), (8), and $P_{cj}[P^{\Pi}_{SIR}]$ with considering (12)
  Acquiring j if P^{Π}_{SIR} and $P_{cj}[P^{\Pi}_{SIR}]$ of an annulus are minimum;
  Organize sorted min to max of probabilities for k=1:6; (add sorted $P^{\Pi}_{SIR_j}$, k, j in a matrix)
  for k=1:1:6; **do**
    The width of annulus j with $P^{\Pi}_{SIR_k}$ is reduced with respect to (21).
    This reduced value is added to the width of the inner annulus $j-1$ (22).
    Density calculation (ρ_j) for the annuluses due to (19)
    Keep fixed the width of annulus j (r_j)
    if $\rho_j > \lambda$ / 3.
    $k = k+1$;
  end for
  $m = m+1$;
end while
The width of SF-annulus is achieved

with numerical limitations. When special devices transmit special nodes, no other device will be allowed to transmit simultaneously in the same annulus. A single gateway LoRa network with SFs allocated employing the SPD method is presented in Figure 2. In this figure, special devices are shown with pink color. The SPD scheme is represented in Algorithm 1.

8 Results and Discussion

The proposed SPD and the EIB scheme are evaluated and compared with regard to scalability with success and coverage probability metrics via simulations. The SPD is run on MATLAB R2019b. The 1500 end devices are randomly distributed due to the Poisson point process in an assumed circle with radius R. The success probability of uplink transmission in the gateway is computed by moving an end device from the most inner to the outer of annuluses.

The success probability of transmissions is evaluated first for the SIR of signal more than the SIR threshold for both methods under concurrent devices interfering as inter-SF and co-SF interferences. Second, the SNR of the signal is more than the SNR threshold for evaluating the success probability under AWGN. Available SFs are 7 to 12. The duty cycle α detects simultaneous transmitting devices. The utilized parameter configure are presented in Table 2.

The SPD method is run in multi-annulus networks and based on this method, the SFs assigned to devices in annuluses. The allocated SFs to annuluses are from inner to outer in order 7 to 12. The SF-dependent

Table 2. THE SF-Dependent SNR Thresholds.

Parameter	Symbol	Value
Bandwidth	B	125 kHz
Carrier frequenc	f_c	868.10 MHZ
Noise power density	N_0	-174 dBm/Hz
Noise figure	NF	6 dB
Transmitting power	P_t	14 dBm
Duty cycle	α	0.33%
Pathloss exponent	η	3

SNR thresholds are used the same as [12]. Then, the performance of the method with respect to the coverage probability metric is computed with varying the number of end devices concerning the joint impact of inter-SF and co-SF interferences performance in the clean and AWGN conditions is measured.

8.1 Success Probability

Figure 3 demonstrates the success probability of the defined LoRa network with a single gateway in the existence of inter-SF and co-SF interferences (P^{Π}_{SIR}) for the proposed SPD scheme and the compared method EIB.

In this simulation result, $R = 10km$ is assumed the same as [12]. P^{Π}_{SIR} curve shows that as the device distance from the gateway or base station is longer in both SPD and EIB methods, the probability of success degrades.

This is because of the impact of path loss and fading on the desired signals. The width of all annuluses in EIB are identical with each other, while their width in SPD is specified with respect to (7) and (8) for determining probability and the equations (20) to (23) repeatedly at the beginning of the network configuration. Iterations continue until the all annulus success probability is more than 0.4 unless the density of that annulus is one-third of the total density.

In this case, the width for that SF remains fixed and will be removed from subsequent rounds to determine the SF region width. As can be seen in two curves, in general, as the SFs grows, the joint interference increases, and as a result, the success probability decreases. The SPD performs better than EIB at all distances, as shown in Figure 3.

The SPD success probability under joint inter-SF

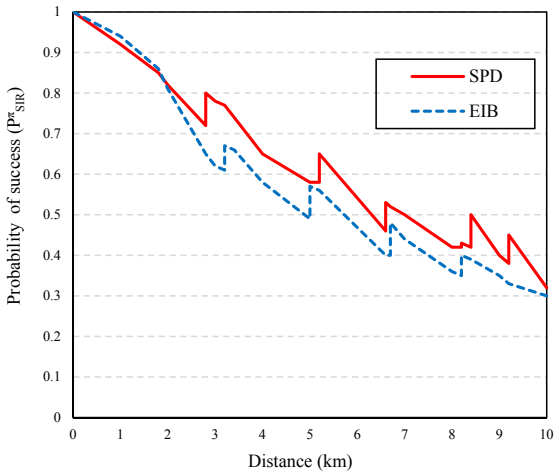

Figure 3. Impact of SF-allocation on success probability under inter-SF and co-SF interference (N=1500).

and co-SF interference P_{SIR}^{Π} of SPD has an averagely of 13.20% improvement over the EIB. The SNR-based success probability (P_{SNR}) under AWGN has better performance than EIB, as shown in Figure 4. SPD selects a lower SF than EIB at higher distances; that is the reason for more drop of SNR-based success probability of the EIB method. The equality of P_{SNR} at the cell boundary is because of utilizing the same SF by methods.

As shown in Figure 4, the curve's line for higher SFs in SPD is shorter than EIB, such as SF 12. Higher SFs result in higher processing, and hence it decreases SNR for correct receiving at the receiver, resulting in lower success probability under AWGN. Therefore P_{SIR} in SPD is higher than EIB.

8.2 Coverage Probability Analysis

Another primary metric to be considered for scalability is joint coverage probability $P_c[P_{SNR}.P_{SIR}^{\Pi}]$. According to (18), the joint coverage probability under the AWGN, inter-SF, and co-SF interferences is simulated and depicted in Figure 5. These simulation results demonstrate the LoRa scalability with growing the number of devices for radius $R = 10km$. In both SPD and EIB methods, the probability of coverage degrades exponentially with the increase in end devices; because SINR will be reduced due to equation (16).

In addition, inter-SF and co-SF interferences increase. Indeed, with the increase in the number of end devices, the number of concurrent transmissions enhances and increases the outage probability. In SINR as (16), the AWGN component is the variance σ^2 that determines the SINR value with interferences.

About the case of inter-SF interference, whatever

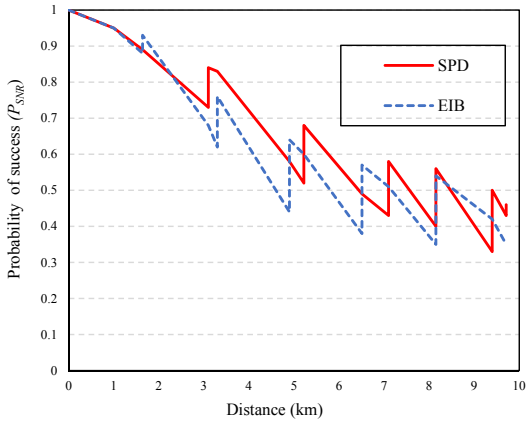

Figure 4. Success Probability Under AWGN.

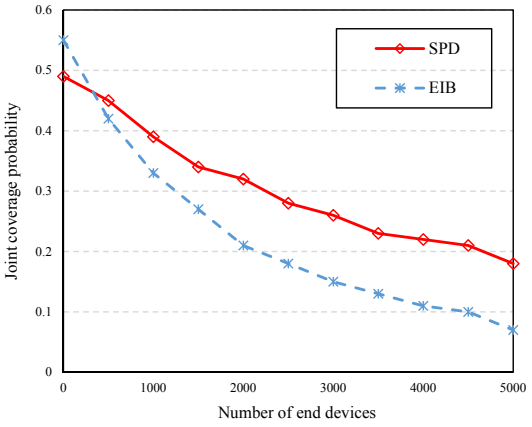

Figure 5. Joint Coverage Probability $P_c[P_{SIR}.P_{SIR}^{\Pi}]$ Under Noise, Interference, and Scalability (R=10 km).

the SF is greater, the SINR threshold will increase as a matrix (17). The downward trend slope in the SPD curve is less than the EIB. One object of SPD is that the annulus with more devices becomes narrower, coverage doesn't drop much at higher SFs. With this process, SPD reduces the dependency on the annulus device density.

The width of annuluses is computed due to success probability given as (7) and device density in each annulus that is given as (19) in the LoRa network region. If the annulus is denser in which the success probability is lower, the width of annulus reduces.

Therefore, the coverage probability is enhanced. The joint coverage probability concerning AWGN, inter-SF, and co-SF interference in the SPD method is higher than the EIB method. As shown in Figure 5, coverage probability in SPD limits the scalability of a LoRa network less than EIB. Consequently, the coverage probability is smaller when the LoRa network is denser.

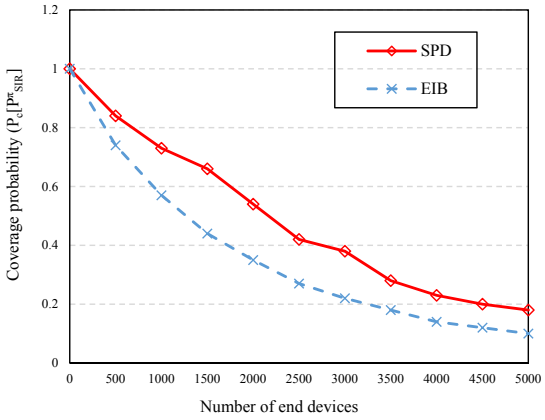

Figure 6. SIR-Based Coverage Probability and Scalability (R=12 km).

The coverage probability metric obtained due to (12) includes inter-SF and co-SF interferences. According to (12), the coverage probability under inter-SF and co-SF $P_c[P^{\Pi}_{SIR}]$ is evaluated using the success probability. For this reason, it is directly related to the success value in each SF.

As shown in Figure 6, SIR-based coverage probability curves of SPD and EIB methods decreased exponentially with the growing number of end devices, showing the scalability in $R = 12km$. Also, the SIR-based coverage probability of SPD outperforms EIB. Considering (12), in the dense annulus with less success probability, the width decreases. As a result, the coverage probability increases.

8.3 Discussion

EIB has an equal-interval-based annulus width selection. The end devices use the lowest SF 7 in the inner annulus near to gateway, and SF increases by one step for outer annuluses. It is shown the interference in higher SFs is more than that in lower SFs [14], and the receiver sensitivity is lower with higher SFs. Hence higher SFs require lower SNR.

Therefore, in both methods SPD and EIB, SF improves the performance at the inner boundary of every annulus. The saw-tooth and jumping trend in the success probability in Figures 3 and 4 observed in both methods is because of switching to a higher SF region and next annulus. The position of saw-tooth behavior on the SPD curve demonstrates unequal SF annuluses.

At the first configuration, the width of annuluses in SPD has been determined based on the relationship between success probability and density mentioned in (20) to (23). Also, SF boundaries are equal, and SPD reduces the impact of EIB interference, which has equal annuluses. Thus, it has better performance than EIB when the network is evaluated with the SPD method in terms of success probability under inter-SF and co-SF interferences conditions. In (20) to (23), the density limits the width of annuluses. Finally, the width of denser annuluses is less.

The scalability is directly related to covering the devices in the network and achieving and demodulating the packets correctly. The success of packet receiving correctly also is dependent on inter-SF and co-SF interference created during the signal transmission by other end devices as interferers that transmit at the same time. The SPD success probability is more than the EIB, so SPD's scalability and reliability after SF-allocation also increase. The location of the saw-tooth shape in success probabilities curves shows that the boundaries of SFs are not equal. Since the inner ring width enhances, in the SF7 region, the success probability degrades a little, as shown in Figure 3.

In the very dense environment LoRa networks, the interference causes a degradation in packet interfering or success receiving performance. In addition to considering the total radius of the circular deployment, the effect of background noise must be considered for the scalability analysis in the conditions of bounded transmitting power of end devices and signal propagation.

The success probability in AWGN is proportional to the SNR thresholds that are fixed in each annulus. With the increase of SNR threshold, the success probability in AWGN reduces, assuming other parameters remain constant due to (6). Therefore, as the width of the annulus decreases in the higher SFs, SPD outperforms EIB, as shown in Figure 4. The SNR-based success probability is independent of LoRa network density.

The higher coverage probability makes more devices accessible for the gateway. A threshold has been defined for SIR and SINR of the received signal in the gateway. As mentioned before, these thresholds determine the probability of success communicating and decoding in the gateway. As it is clear from the matrix (17), these thresholds are more with the increase in SF. Hence this probability of success to communicate correctly is reduced. Since the higher SF's area is narrower, success probability in wider areas grows.

The SPD determines the SF region based on primitive computations of success probability and intensity. By selecting the annulus widths step by step according to (20) to (23), the width varies according to the probability improvement compared to the initial state, EIB structure. Therefore, SPD gets better results. On the other hand, developed success probability improves the coverage probability with both inter-SF and co-SF

interferences ($P_c[P_{SIR}^{\Pi}]$) and under joint AWGN and interference ($P_c[P_{SNR}.P_{SIR}^{\Pi}]$).

According to Figures 5 and 6, the probability of coverage in EIB has more dependency on the density than the SPD method. Curve's trend in Figure 6 is similar to that of in Figure 5. Joint inter-SF and co-SF interference affect the decline of curves in Figures 5 and 6.

9 Conclusions

One of the parameters that impact the scalability of the LoRa network is the spreading factor. This paper proposes a method of allocating SF based on success probability under inter-SF interference and co-SF interference associated with scalability. Also, this method depends on the density. Then the proposed method is analyzed by evaluating success and coverage probability metrics. In the very dense establishment of networks, performance decline is the result of interference, which is the most important reason. To solve this deterioration, the SPD method has been proposed. The proposed SPD method is a novel multi-annulus scheme with different widths of assigned SF. The SPD is based on the success probability under the cumulative impact of inter-SF and co-SF interferences. Then, the density of annuluses is considered.

These two parameters allocate the SFs independently. The total density of LoRa-cell also impacts the SF-allocation. The algorithm is run at the first of the network configuration. It is compared with the EIB method via simulations to confirm the better performance and prove that the LoRa network structure configured with the SPD method is more reliable and scalable. The used metrics for assessment are success probability under inter-SF and co-SF interferences, success probability under AWGN, and coverage probability in the existence of inter-SF and co-SF interferences in the clean and AWGN environment.

The simulation results approved the effectiveness of SPD with regard to success probability and coverage probability metrics in the scalability analysis. In the proposed SPD method, the network performance under inter-SF and co-SF interferences with regard to success probability has improved 13.20% over compared method EIB. According to the simulation results, SPD also outperforms the EIB in terms of coverage probability.

Future works are to study the LoRa networks with multiple gateways. These networks are investigated in terms of scalability. Also, it will try to use other parameter settings of LoRa to check the number of devices covered by the network.

References

[1] M. Sain, Y. J. Kang, and H. J. Lee. Survey on security in Internet of Things: State of the art and challenges. In *2017 19th International Conference on Advanced Communication Technology (ICACT)*, pages 699–704. IEEE, 2017. ISBN 978-89-968650-9-4. doi:10.23919/ICACT.2017.7890183.

[2] G. A. Akpakwu, B. J. Silva, G. P. Hancke, and A. M. Abu-Mahfouz. A survey on 5G networks for the Internet of Things: Communication technologies and challenges. *IEEE Access*, 6:3619–3647, 2017. ISSN 2169-3536. doi:10.1109/ACCESS.2017.2779844.

[3] J. Chen, K. Hu, Q. Wang, Y. Sun, Z. Shi, and S. He. Narrowband Internet of Things: Implementations and Applications. *IEEE Internet of Things Journal*, 4(6):2309–2314, 2017. ISSN 2327-4662. doi:10.1109/JIOT.2017.2764475.

[4] A. Lavric, A. I. Petrariu, and V. Popa. Long Range SigFox Communication Protocol Scalability Analysis Under Large-Scale, High-Density Conditions. *IEEE Access*, 7: 35816 – 35825, 2019. ISSN 2169-3536. doi:10.1109/ACCESS.2019.2903157.

[5] P. Gkotsiopoulos, D. Zorbas, and C. Douligeris. Performance Determinants in LoRa Networks: A Literature Review. *IEEE Communications Surveys & Tutorials*, 23(3):1721 – 1758, 2021. doi:10.1109/COMST.2021.3090409.

[6] U. Raza, P. Kulkarni, and M. Sooriyabandara. Low Power Wide Area Networks: An Overview. *IEEE Communications Surveys & Tutorials*, 19(2):855 – 873, 2017. doi:10.1109/COMST.2017.2652320.

[7] F. Adelantado, X. Vilajosana, P. Tuset-Peiro, B. Martinez, J. Melia-Segui, and T. Watteyne. Understanding the Limits of LoRaWAN. *IEEE Communications Magazine*, 55(9):34 – 40, 2017. ISSN 0163-6804. doi:10.1109/MCOM.2017.1600613.

[8] J. Haxhibeqiri, F. Van den Abeele, I. Moerman, and J. Hoebeke. LoRa Scalability: A Simulation Model Based on Interference Measurements. *Sensors*, 17(6), 2017. ISSN 1424-8220. doi:10.3390/s17061193.

[9] A. Lavric and V. Popa. Performance Evaluation of LoRaWAN Communication Scalability in Large-Scale Wireless Sensor Networks. *Wireless Communications and Mobile Computing*, 2018, 2018. doi:10.1155/2018/6730719.

[10] C. Pham, A. Bounceur, L. Clavier, U. Noreen, and M. Ehsan. Radio channel access challenges in LoRa low-power wide-area networks. *LPWAN Technologies for IoT and M2M Applications*, 2020:65–102, 2020. doi:10.1016/B978-0-12-

818880-4.00004-1.

[11] Y. Jiang, L. Peng, A. Hu, S. Wang, Y. Huang, and L. Zhang. Physical layer identification of LoRa devices using constellation trace figure. *EURASIP Journal on Wireless Communications and Networking*, 2019(1):1–11, 2019. doi:10.1186/s13638-019-1542-x.

[12] A. Mahmood, E. Sisinni, L. Guntupalli, R. Rondón, S. A. Hassan, and M. Gidlund. Scalability Analysis of a LoRa Network Under Imperfect Orthogonality. *IEEE Transactions on Industrial Informatics*, 15(3):1425 – 1436, 2019. ISSN 1551-3203. doi:10.1109/TII.2018.2864681.

[13] A. Waret, M. Kaneko, A. Guitton, and N. El Rachkidy. LoRa Throughput Analysis With Imperfect Spreading Factor Orthogonality. *IEEE Wireless Communications Letters*, 8(2):408 – 411, 2019. ISSN 2162-2337. doi:10.1109/LWC.2018.2873705.

[14] D. Croce, M. Gucciardo, I. Tinnirello, D. Garlisi, and S. Mangione. Impact of Spreading Factor Imperfect Orthogonality in LoRa Communications. In *International Tyrrhenian Workshop on Digital Communication*, pages 165–179. Springer, 2017. ISBN 978-3-319-67638-8. doi:10.1007/978-3-319-67639-5_13.

[15] M. C. Bor, U. Roedig, T. Voigt, and J. M. Alonso. Do LoRa Low-Power Wide-Area Networks Scale? In *Proceedings of the 19th ACM International Conference on Modeling, Analysis and Simulation of Wireless and Mobile Systems*, page 59–67. ACM, 2016. doi:10.1145/2988287.2989163.

[16] J. Lim and Y. Han. Spreading Factor Allocation for Massive Connectivity in LoRa Systems. *IEEE Communications Letters*, 22(4):800 – 803, 2018. ISSN 1089-7798. doi:10.1109/LCOMM.2018.2797274.

[17] F. Van den Abeele, J. Haxhibeqiri, I. Moerman, and J. Hoebeke. Scalability Analysis of Large-Scale LoRaWAN Networks in ns-3. *IEEE Internet of Things Journal*, 4(6):2186 – 2198, 2017. ISSN 2327-4662. doi:10.1109/JIOT.2017.2768498.

[18] O. Georgiou and U. Raza. Low Power Wide Area Network Analysis: Can LoRa Scale? *IEEE Wireless Communications Letters*, 6(2):162 – 165, 2017. ISSN 2162-2337. doi:10.1109/LWC.2016.2647247.

[19] V. Di Vincenzo, M. Heusse, and B. Tourancheau. Improving Downlink Scalability in LoRaWAN. In *ICC 2019 - 2019 IEEE International Conference on Communications (ICC)*, pages 1–7. IEEE, 2019. ISBN 978-1-5386-8088-9. doi:10.1109/ICC.2019.8761157.

[20] C. Kim, J. Kim, J. Kwak, K. Kim, and W. Seok. Occupancy-balancing downlink transmission for enhancing scalability of LoRa networks. *International Journal of Distributed Sensor Networks*, 16(12), 2020. ISSN 1550-1477. doi:10.1177/1550147720979279.

[21] V. Di Vincenzo, M. Heusse, and B. Tourancheau. EWS: Exponential Windowing Scheme to Improve LoRa Scalability. In *IEEE Transactions on Industrial Informatics*, pages 1–7. IEEE, 2019. ISBN 978-1-5386-8088-9. doi:10.1109/ICC.2019.8761157.

[22] Q. Cai and J. Lin. Improving the Scalability of LoRa Networks Through Dynamical Parameter Set Selection. In *China Conference on Wireless Sensor Networks*, pages 3–18. Springer, 2019. ISBN 978-981-15-1784-6. doi:10.1007/978-981-15-1785-3_1.

[23] T. Polonelli, D. Brunelli, A. Marzocchi, and L. Benini. Slotted ALOHA on LoRaWAN-Design, Analysis, and Deployment. *Sensors*, 19(4):838, 2019. ISSN 1424-8220. doi:10.3390/s19040838.

[24] B. Reynders, Q. Wang, P. Tuset-Peiro, X. Vilajosana, and S. Pollin. Improving Reliability and Scalability of LoRaWANs Through Lightweight Scheduling. *IEEE Internet of Things Journal*, 5(3):1830 – 1842, 2018. ISSN 2327-4662. doi:10.1109/JIOT.2018.2815150.

[25] J. Haxhibeqiri, I. Moerman, and J. Hoebeke. Low Overhead Scheduling of LoRa Transmissions for Improved Scalability. *IEEE Internet of Things Journal*, 6(2):3097 – 3109, 2018. ISSN 2327-4662. doi:10.1109/JIOT.2018.2878942.

[26] A. Lavric and V. Popa. Performance Evaluation of LoRaWAN Communication Scalability in Large-Scale Wireless Sensor Networks. *Wireless Communications and Mobile Computing*, 2018, 2018. doi:10.1155/2018/6730719.

[27] M. O. Ojo, D. Adami, and S. Giordano. Experimental Evaluation of a LoRa Wildlife Monitoring Network in a Forest Vegetation Area. *Future Internet*, 13(5), 2021. doi:10.3390/fi13050115.

[28] S. Mohammadi and G. Farahani. Scalability Analysis of a LoRa Network Under Co-SF and Inter-SF Interference in Large-scale IoT Applications. In *2021 5th International Conference on Internet of Things and Applications (IoT)*, pages 1–6. IEEE, 2021. ISBN 978-1-6654-4448-4. doi:10.1109/IoT52625.2021.9469719.

[29] M. Aljuaid and H. Yanikomeroglu. Investigating the Gaussian Convergence of the Distribution of the Aggregate Interference Power in Large Wireless Networks. *IEEE Transactions on Vehicular Technology*, 59(9):4418 – 4424, 2010. ISSN 0018-9545. doi:10.1109/TVT.2010.2067452.

[30] M. Haenggi and R. K. Ganti. *Interference in large wireless networks*. Now Publishers Inc, 2009.

[31] R. G. Gallager. Discrete Stochastic Processes. *OpenCourseWare: Massachusetts Institute of*

Technology, 2011.

[32] R. W. Heath, M. Kountouris, and T. Bai. Modeling Heterogeneous Network Interference Using Poisson Point Processes. *IEEE Transactions on Signal Processing*, 61(16):4114 – 4126, 2013. ISSN 1941-0476. doi:10.1109/TSP.2013.2262679.

[33] Semtech. LoRa modulation basics, AN1200.22. 2015.

[34] D. Croce, M. Gucciardo, S. Mangione, G. Santaromita, and I. Tinnirello. Impact of LoRa Imperfect Orthogonality: Analysis of Link-Level Performance. *IEEE Communications Letters*, 22(4):796 – 799, 2018. ISSN 1089-7798. doi:10.1109/LCOMM.2018.2797057.

[35] A. Hoeller, R. Souza Demo, O. L. A. López, H. Alves, M. de Noronha Neto, and G. Brante. Analysis and Performance Optimization of LoRa Networks With Time and Antenna Diversity. *IEEE Access*, 6:32820 – 32829, 2018. ISSN 2169-3536. doi:10.1109/ACCESS.2018.2839064.

[36] A. Farhad, D. Kim, and J. Pyun. Resource Allocation to Massive Internet of Things in LoRaWANs. *Sensors*, 20(9):2645, 2020. ISSN 1424-8220. doi:10.3390/s20092645.

Solmaz Mohammadi was born in Tehran, Iran in 1989. She received her B.Sc degree in electrical engineering from Shariaty Technical College, Tehran, Iran, in 2012 and an M.Sc degree in electrical engineering from Electrical Engineering and Information Technology Department, Iranian Research Organization for Science and Technology (IROST), Tehran, Iran in 2020. She is interested and works on IoT, especially WSN and LPWAN includes NB-IoT, LTE-M, LoRa, SigFox, and other related technologies.

Gholamreza Farahani was born in Shahriyar, Tehran, Iran in 1976. He received his B.Sc degree in electrical engineering from the Sharif University of Technology, Tehran, Iran, in 1998 and M.Sc and Ph.D. degrees in electrical engineering from Amirkabir University of Technology (Polytechnic), Tehran, Iran in 2000 and 2006, respectively. Currently, he is an associate professor with the Electrical Engineering and Information Technology Department, Iranian Research Organization for Science and Technology (IROST), Tehran, Iran. His research interests include wireless sensor networks and data communication in LPWAN.